

Suppression of weak antilocalization in an $\text{Al}_x\text{Ga}_{1-x}\text{N}/\text{GaN}$ two-dimensional electron gas by an in-plane magnetic field

S. Cabañas, Th. Schäpers,* N. Thilloßen, N. Kaluza, V. A. Guzenko, and H. Hardtdegen
*Institute of Bio- and Nanosystems (IBN-1) and Virtual Institute of Spin Electronics (VISel), Research Centre Jülich GmbH,
 52425 Jülich, Germany*

(Received 24 January 2007; revised manuscript received 6 April 2007; published 22 May 2007)

We studied the suppression of weak antilocalization in an $\text{Al}_x\text{Ga}_{1-x}\text{N}/\text{GaN}$ two-dimensional electron gas in the presence of an additional in-plane magnetic field. By comparing our experimental data to a theoretical model, we concluded that the suppression can be attributed mainly to the Zeeman effect, while the contribution due to disorder at the $\text{Al}_x\text{Ga}_{1-x}\text{N}/\text{GaN}$ heterointerface is considerably smaller. Furthermore, our results give further evidence for the value of spin-orbit scattering length determined from weak antilocalization measurements.

DOI: [10.1103/PhysRevB.75.195329](https://doi.org/10.1103/PhysRevB.75.195329)

PACS number(s): 73.20.Fz, 73.43.Qt, 72.25.Rb, 73.61.Ey

Despite the fact that GaN is a large-band-gap material, clear indications of the presence of a spin-orbit coupling were recently observed in AlGaN/GaN two-dimensional electron gases (2DEGs).¹⁻⁹ This result is somewhat astonishing, since usually pronounced spin-orbit coupling is expected in low-band-gap semiconductors, i.e., InAs or InGaAs. The latter is due to the fact that the strength of spin-orbit coupling increases with decreasing band-gap energy and increasing valence-band splitoff energy, as is the case for the semiconductor materials given above.¹⁰ Nevertheless, a spin-orbit energy splitting was observed in AlGaN/GaN 2DEGs. It can be attributed to the large sheet electron concentration and to the large internal piezoelectric fields. The latter are a result of the lower symmetry of the wurtzite crystal lattice, which is the stable configuration of AlGaN/GaN heterostructures, compared to the zinc-blende structure of most other III-V semiconductors.

Information on the strength of spin-orbit coupling in AlGaN/GaN 2DEGs can be obtained, e.g., by analyzing the characteristic beating pattern in Shubnikov–de Haas oscillations¹⁻⁴ or by the investigation of the circular photogalvanic effect.⁵ However, by using the first approach, a large spread of the spin-orbit coupling parameter was found, with some values considerably larger than the theoretically estimated ones.¹¹ Another viable way is to analyze weak antilocalization.^{3,6-9} Here, in the presence of spin-orbit coupling, the quantum-mechanical interference of electrons propagating on time-reversed paths results in an enhanced conductance at zero magnetic field.¹²⁻¹⁴ Compared to the studies of Shubnikov–de Haas oscillations, the analysis of weak antilocalization led to more consistent results. In fact, in all studies on 2DEGs with only a single conductive subband occupied, a characteristic spin-orbit field B_{so} close to 2 mT was reported.⁶⁻⁹ The quantity B_{so} is a measure of the strength of spin-orbit coupling.

In order to deepen our knowledge on spin-related effects in the transport properties of AlGaN/GaN heterostructures, we conducted weak antilocalization measurements with an additional magnetic field B_{\parallel} applied parallel to the plane of the 2DEG. The effect of B_{\parallel} on the magnetoconductivity is expected to be twofold. First, the parallel field results in an additional Zeeman energy splitting according to $E_z = g\mu_B B_{\parallel}$,

with g the electron gyromagnetic factor and μ_B the Bohr magneton. As pointed out by Mal'shukov *et al.*,^{15,16} the Zeeman interaction causes a suppression of the weak antilocalization peak. Experimentally, a suppression of weak antilocalization in $\text{Ga}_x\text{In}_{1-x}\text{As}$ quantum wells was observed by Minkov *et al.*¹⁷ and Meijer *et al.*^{18,19} As a second effect of B_{\parallel} , potential fluctuations due to disorder in the channel, i.e., induced by charged impurities or by interface roughness at the heterojunction, can give rise to a suppression of interference effects.^{17,20-25}

In this paper, we report on the weak antilocalization measurement of AlGaN/GaN 2DEGs with an in-plane field B_{\parallel} applied, in addition. We will elucidate to which extent the Zeeman interaction and potential fluctuations due to disorder contribute to the suppression of weak antilocalization. The Zeeman contribution was considered by taking the known g factor for GaN into account,²⁶ while the effect of the disorder contribution is estimated based on the experimentally determined surface morphology of the layer system. The measurements in a parallel magnetic field allowed us to give further evidence for the strength of spin-orbit coupling determined by weak antilocalization.

Two different polarization-doped $\text{Al}_x\text{Ga}_{1-x}\text{N}/\text{GaN}$ heterostructures were grown by metal-organic vapor phase epitaxy on a (0001) Al_2O_3 substrate. Both layer sequences consisted of a 3- μm -thick GaN layer followed by an $\text{Al}_{0.15}\text{Ga}_{0.85}\text{N}$ top layer with thicknesses of 70 and 35 nm for samples A and B, respectively. A schematic of the layer sequence of sample A is depicted in Fig. 1 (inset). All layers were nominally undoped. Hall bar structures with a width of 200 μm and with voltage probes separated by 180 μm were defined by dry mesa etching. Sample B was covered by a Ni/Au gate electrode isolated from the semiconductor surface by a SiO_2 layer.

The samples were measured in a He-3 cryostat equipped with a superconducting coil with a maximum field of 10 T. The standard lock-in technique was employed to determine the magnetoresistance. The first sets of Shubnikov–de Haas measurements were performed in a configuration with the magnetic field aligned perpendicularly to the plane of the 2DEG. For the subsequent measurements in an in-plane magnetic field B_{\parallel} , the samples were mounted with the plane

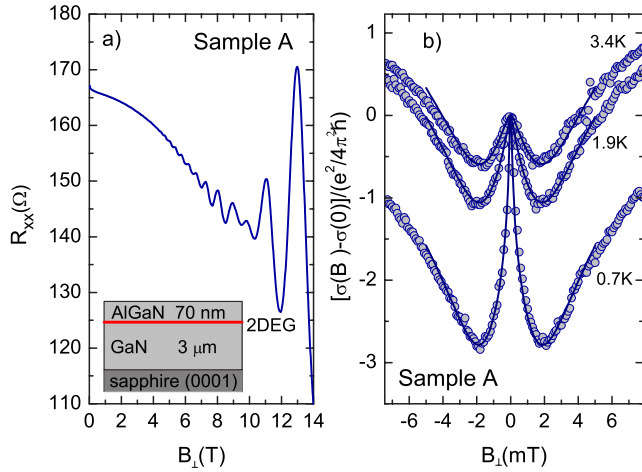


FIG. 1. (Color online) (a) Magnetoresistance R_{xx} of sample A measured at a temperature of 1.0 K with the magnetic field aligned perpendicularly to the plane of the 2DEG. The inset shows the layer sequence of sample A. (b) Experimental values (\circ) of the quantum correction to the conductivity $\sigma(B_{\perp}) - \sigma(0)$ in units of $e^2/4\pi^2\hbar$ vs B_{\perp} at temperatures of 0.7, 1.9, and 3.4 K (sample A). Full lines show the fit to the experimental data using the ILP model (Ref. 27).

of the 2DEG aligned along the field of the 10 T magnet. A pair of small superconducting split coils with a maximum field of 20 mT was used to apply a perpendicular magnetic field B_{\perp} . Owing to the small size of the samples compared to the diameter of the split coils, inhomogeneities of B_{\perp} could be neglected.

The presence of a 2DEG at the AlGaIn/GaN interface can be deduced from the observance of pronounced Shubnikov-de Haas oscillations, as shown in Fig. 1(a) for sample A. From the $(1/B)$ fast Fourier transform of the oscillations in $R_{xx}(B_{\perp})$, a sheet electron concentration of $n = 3.51 \times 10^{12} \text{ cm}^{-2}$ was extracted. Only a single subband was occupied. Temperature-dependent measurements confirmed that the electron concentration remains constant in the temperature range from 0.5 to 3.4 K. From the resistance at $B_{\perp} = 0$, a mobility of $\mu = 8530 \text{ cm}^2/\text{V s}$ was determined, resulting in a transport mean free path l_{tr} of 260 nm and a diffusion constant D of $0.033 \text{ m}^2/\text{s}$. From corresponding measurements for sample B at zero gate voltage, $n = 4.21 \times 10^{12} \text{ cm}^{-2}$ and $\mu = 7390 \text{ cm}^2/\text{V s}$ were extracted, resulting in $l_{tr} = 250 \text{ nm}$ and $D = 0.034 \text{ m}^2/\text{s}$. At gate voltages of -0.5 and -1.0 V, the electron concentrations are reduced to 3.85×10^{12} and $3.53 \times 10^{12} \text{ cm}^{-2}$, respectively. At all gate voltages, only a single subband was occupied.

In the following, we will focus on the transport properties close to zero magnetic field. In Fig. 1(b) the quantum correction to the conductivity $\sigma(B_{\perp}) - \sigma(0)$ of sample A is shown for three different temperatures. The pronounced peak at zero magnetic field can be attributed to weak antilocalization, being a clear indication of the presence of spin-orbit coupling.¹² At ± 2 mT, the slope of $\sigma(B_{\perp}) - \sigma(0)$ changes sign, indicating the transition from weak antilocalization to weak localization at sufficiently large magnetic fields. Since the effects observed here originate from electron interference, the decrease of the phase coherence length l_{ϕ} with

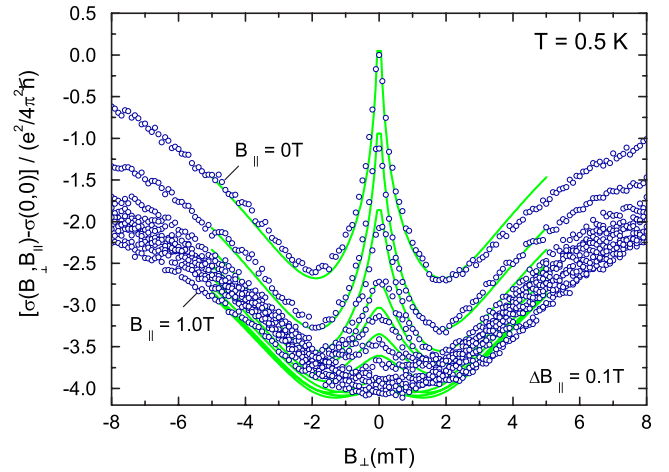


FIG. 2. (Color online) Experimental values (\circ) of the quantum correction to the conductivity $[\sigma(B_{\perp}, B_{\parallel}) - \sigma(0, 0)] / (e^2/4\pi^2\hbar)$ of sample A as a function of a perpendicular magnetic field B_{\perp} . The in-plane magnetic field B_{\parallel} was changed as a parameter from 0 to 1.0 T in steps of 0.1 T. The full line shows the fit to the model of Mal'shukov *et al.* (Ref. 15).

temperature results in a corresponding decrease of the weak antilocalization peak at $B_{\perp} = 0$.⁷ The slight asymmetry of the conductivity with respect to the magnetic-field sign is attributed to a small asymmetry in the sample geometry.

In order to obtain information on the spin-orbit scattering length l_{so} and on the phase coherence length l_{ϕ} , the experimental curves plotted in Fig. 1(b) were fitted by using the model of Iordanskii, Lyanda-Geller, and Pikus (ILP).²⁷ Only the k -linear Rashba contribution was assumed, while any contribution due to the crystal anisotropy was neglected.⁷ Under this condition, the quantum corrections to the conductivity depend on three characteristic fields, i.e., B_{tr} , B_{ϕ} , and B_{so} . The first parameter B_{tr} , which is defined by $\hbar/2el_{tr}^2$, can be determined directly from l_{tr} as given above. Note that the ILP model is only valid for $B < B_{tr}$, in our case: $B_{tr} = 5$ mT. The remaining two characteristic fields $B_{\phi} = \hbar/4eD\tau_{\phi}$ and $B_{so} = \hbar/4eD\tau_{so}$ were extracted from the fit to the experimental data. Here, τ_{ϕ} and τ_{so} are the phase breaking time and spin-orbit scattering time, respectively. At 1.0 K, the best fit was achieved for $H_{\phi} = 7 \mu\text{T}$ and $H_{so} = 1.6$ mT. The values of τ_{ϕ} and τ_{so} correspond to a phase coherence length $l_{\phi} = \sqrt{D\tau_{\phi}}$ of $3.7 \mu\text{m}$ and a spin-orbit scattering length $l_{so} = \sqrt{D\tau_{so}}$ of 300 nm, respectively.

If an additional in-plane magnetic field B_{\parallel} is applied, the height of the weak antilocalization peak decreases. This can be seen in Fig. 2, where B_{\parallel} was changed as a parameter from 0 to 1.0 T. A full suppression of the weak antilocalization peak is reached at $B_{\parallel} = 1.0$ T. However, the slope of $\sigma(B_{\perp}, B_{\parallel}) - \sigma(0, 0)$ for $|B_{\perp}| \geq 2$ mT attributed to weak localization is basically unchanged if an in-plane field is applied.

As outlined above, an in-plane magnetic field can cause a suppression of weak antilocalization either due to the Zeeman effect or due to disorder in the channel. Since in our case only a single subband is occupied, finite thickness effects were neglected.^{23,25,28,29} In order to quantify the effect of the Zeeman and disorder contributions, we followed the

approach of Mal'shukov *et al.*^{15,16} Here, the quantum interference corrections to the conductance is divided into two contributions.^{27,29} First, the triplet part F_t , representing scattered states with a total angular momentum of 1. The triplet channel contributes negatively to the interference corrections of conductivity, i.e., lowers the conductivity. The second term is the singlet part F_s , representing scattering states with zero total angular momentum. The singlet channel contributes positively to the conductivity correction, thus increasing the conductivity. The dependence of the quantum-mechanical correction to the conductivity on a combined perpendicular and in-plane magnetic field can be expressed as¹⁵⁻¹⁷

$$\sigma(B_{\perp}, B_{\parallel}) - \sigma(0, B_{\parallel}) = \frac{e^2}{4\pi^2\hbar} \left[F_t \left(\frac{B_{\phi,t}}{B_{\perp}}, \frac{B_{so}}{B_{\perp}} \right) - F_s \left(\frac{B_{\phi,s}}{B_{\perp}}, \frac{B_{so}}{B_{\perp}} \right) \right]. \quad (1)$$

Here, the characteristic fields representing the phase breaking in the triplet and singlet contributions are defined by $B_{\phi,t} = \hbar/4eD\tau_{\phi,t}$ and $B_{\phi,s} = \hbar/4eD\tau_{\phi,s}$, respectively. For the triplet channel, the effective phase breaking rate is enhanced by the contribution due to the presence of disorder in the channel: $1/\tau_{\phi,t} = 1/\tau_{\phi} + 1/\tau_d$, where $1/\tau_{\phi}$ is the phase breaking rate at $B_{\parallel}=0$. The additional rate $1/\tau_d$, given by^{16,22,23,25}

$$\frac{1}{\tau_d} = \frac{4eD}{\hbar} \gamma_d B_{\parallel}^2, \quad (2)$$

represents the contribution due to disorder. The parameter γ_d is a measure of the effect of the disorder due to charged impurities or due to interface roughness. The phase breaking rate of the singlet state, $1/\tau_{\phi,s} = 1/\tau_{\phi} + 1/\tau_d + 1/\tau_z$, is additionally enhanced by the Zeeman contribution $1/\tau_z$ given by^{15,16}

$$\frac{1}{\tau_z} = \frac{\tau_{so}}{\hbar^2} (g\mu_B B_{\parallel})^2. \quad (3)$$

Here, for τ_{so} the value at $B_{\parallel}=0$ has to be taken.

In order to obtain information to what extent the two mechanisms discussed above contribute to the suppression of the weak antilocalization peak, the experimental curves at various in-plane magnetic fields were fitted using Eq. (1). The corresponding fits are shown in Fig. 2. It turns out that, with regard to the Zeeman contribution, the best fit is obtained for a g factor of 1.95, corresponding to the value determined from electron-spin-resonance experiments on AlGaIn/GaN 2DEGs.²⁶ For τ_{so} , the value extracted from the fit at $B_{\parallel}=0$ using the ILP model was taken. In our case, the Zeeman energy $g\mu_B B_{\parallel}$ is well below \hbar/τ_{so} up to the maximum value of B_{\parallel} , so that Eq. (1) is valid in the whole range of B_{\parallel} .¹⁵ With respect to the disorder contribution, cf. Eq. (2), an optimum value of $2.1 \times 10^{-4} \text{ T}^{-1}$ was found for γ_d . Our fits to the experimental curves at various in-plane magnetic fields confirm that the additional phase breaking owing to the Zeeman effect and to disorder is described well by a B_{\parallel}^2 dependence of $1/\tau_z$ and $1/\tau_d$, respectively. Furthermore, a direct comparison of both rates reveals that, for our sample, phase breaking due to the Zeeman effect is more than a factor of 2 larger. The conclusions drawn for sample A are con-

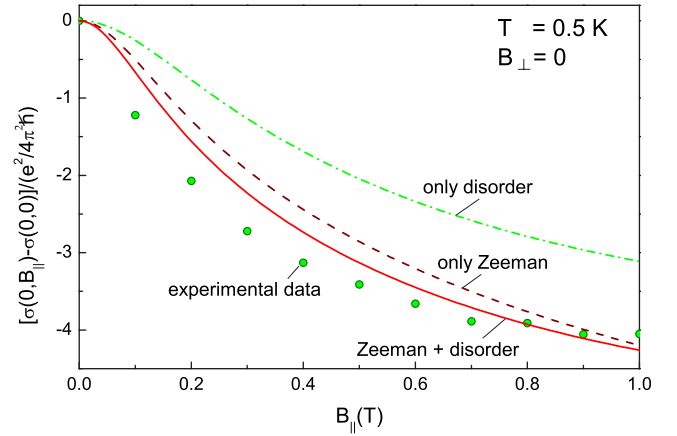


FIG. 3. (Color online) Conductance corrections $[\sigma(0, B_{\parallel}) - \sigma(0, 0)] / (e^2 / 4\pi^2\hbar)$ of sample A as a function of B_{\parallel} at $B_{\perp}=0$ (dots). The full line shows the calculation according to Eq. (4) including the Zeeman and roughness contributions. The dashed and dashed-dotted lines illustrate the case when only the Zeeman contribution or the roughness contribution is assumed, respectively.

firmed by the measurements of sample B; here, for gate voltages of 0, -0.5 , and -1.0 V, the best fits were obtained for the same values of γ_d and g as used for sample A.

In contrast to most other 2DEGs in semiconductor heterostructures in our case, no modulation doping by impurities is required to supply carriers at the AlGaIn/GaN interface. Thus the potential fluctuations due to charged impurities should be small. Since in our structures the carriers are accumulated at the interface due to polarization doping, presumably the major disorder contribution is due to interface roughness. Under this assumption, the value of γ_d obtained from the fit can be compared to values expected from the surface roughness determined from atomic force microscopy. Here, a root-mean-square height \bar{z} of about 0.2 nm was extracted, corresponding to an almost atomically flat surface with monoatomic steps. The correlation length L was approximately $2 \mu\text{m}$ and thus considerably larger than l_{tr} . For this particular case ($L \gg l_{tr}$), Mal'shukov *et al.*¹⁶ gave the following estimate: $\gamma_d \approx (e/\hbar)\bar{z}^2$. With \bar{z} as given above, we obtain a value of $0.6 \times 10^{-4} \text{ T}^{-1}$, being somewhat smaller than the value obtained from the fit.

Further insight into the interplay between the Zeeman and disorder contributions can be gained by analyzing the quantum correction to the conductance at $B_{\perp}=0$ as a function of B_{\parallel} . The corresponding experimental values of $\sigma(0, B_{\parallel}) - \sigma(0, 0)$ for sample A are plotted in Fig. 3. From Eq. (1), Minkov *et al.*¹⁷ derived the following expression in the limit $B_{\perp} \rightarrow 0$:

$$\begin{aligned} \sigma(0, B_{\parallel}) - \sigma(0, 0) = \frac{e^2}{4\pi^2\hbar} \left[2 \ln \left(\frac{B_{\phi,t} + B_{so}}{B_{\phi} + B_{so}} \right) \right. \\ \left. + \ln \left(\frac{B_{\phi,t} + 2B_{so}}{B_{\phi} + 2B_{so}} \right) - \ln \left(\frac{B_{\phi,s}}{B_{\phi}} \right) \right. \\ \left. + S(B_{\phi,t}/B_s) - S(B_{\phi}/B_s) \right]. \quad (4) \end{aligned}$$

Here, $S(x)$ is defined by

$$S(x) = \frac{8}{\sqrt{7+16x}} \left[\arctan\left(\frac{\sqrt{7+16x}}{1-2x}\right) - \pi\Theta(1-2x) \right],$$

with $\Theta(y)$ the Heaviside step function. It can be seen in Fig. 3 that a good agreement with the experimental data is obtained if the values of $B_{\phi,t}$ and $B_{\phi,s}$ are inserted in Eq. (4), which were obtained from the fit shown in Fig. 2. The curves for the case when only the Zeeman effect or only disorder is assumed are also shown in Fig. 3. Obviously, the decrease of $\sigma(0, B_{\parallel}) - \sigma(0, 0)$ with B_{\parallel} is dominated by the Zeeman contribution.

The fact that the contribution of the potential fluctuations due to disorder plays a minor role is confirmed by measurements up to higher values of B_{\parallel} . This aspect is illustrated in Fig. 4, where the corrections to the conductance of sample B at a gate voltage of -0.5 V are plotted. It can be seen that after the weak antilocalization peak is completely suppressed at $B_{\parallel} \approx 1.0$ T, no change in the remaining dip due to weak localization is observed upon a further increase to 3 T. This is in contrast to the theoretically expected damping of the weak localization feature if the disorder contribution is sufficiently large.^{20,22} The narrowing of the weak localization dip upon an increase of B_{\parallel} up to 7 T is not covered by the current theoretical models^{20,22} and was not observed in other material systems.¹⁸

The fits to the experimental data at various values of B_{\parallel} were performed by assuming a constant value for τ_{so} . No increase of τ_{so} with B_{\parallel}^2 was required for a satisfactory fit, in contrast to the results for other material systems.¹⁸ Furthermore, the Zeeman contribution, cf. Eq. (3), is very well described by assuming the value of τ_{so} extracted from the fit at

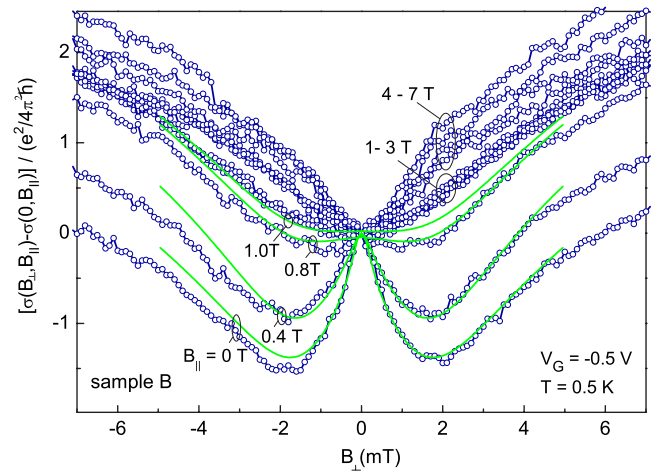


FIG. 4. (Color online) Conductance corrections $[\sigma(B_{\perp}, B_{\parallel}) - \sigma(0, B_{\parallel})]/(e^2/4\pi^2\hbar)$ of sample B as a function of B_{\perp} for B_{\parallel} set to 0, 0.4, and 0.8 T. The following curves correspond to $B_{\parallel} = 1.0$ T up to 7.0 T, with $\Delta B_{\parallel} = 1.0$ T.

$B_{\parallel} = 0$ according to the ILP model. This gives further evidence for a reliable determination of the spin-orbit scattering length by weak antilocalization measurements.

In summary, the peak in the conductance due to weak antilocalization was suppressed by applying a sufficiently large in-plane magnetic field B_{\parallel} . It was found that the suppression can be attributed mainly to the Zeeman contribution. Owing to lack of impurity doping and to the very good interface quality, the disorder contribution plays only a minor role.

*Electronic address: th.schaepers@fz-juelich.de

- ¹I. Lo, J. K. Tsai, W. J. Yao, P. C. Ho, L. W. Tu, T. C. Chang, S. Elhamri, W. C. Mitchel, K. Y. Hsieh, J. H. Huang, H. L. Huang, and W. C. Tsai, *Phys. Rev. B* **65**, 161306(R) (2002).
- ²K. Tsubaki, N. Maeda, T. Saitoh, and N. Kobayashi, *Appl. Phys. Lett.* **80**, 3126 (2002).
- ³J. Lu, B. Shen, N. Tang, D. J. Chen, H. Zhao, D. W. Liu, R. Zhang, Y. Shi, Y. D. Zheng, Z. J. Qiu, Y. S. Gui, B. Zhu, W. Yao, J. H. Chu, K. Hoshino, and Y. Arakawa, *Appl. Phys. Lett.* **85**, 3125 (2004).
- ⁴K. Cho, T.-Y. Huang, H.-S. Wang, M.-G. Lin, T.-M. Chen, C.-T. Liang, and Y. F. Chen, *Appl. Phys. Lett.* **86**, 222102 (2005).
- ⁵W. Weber, S. Ganichev, Z. Kvon, V. Bel'kov, L. Golub, S. Danilov, D. Weiss, W. Prettl, H.-I. Cho, and J.-H. Lee, *Appl. Phys. Lett.* **87**, 262106 (2005).
- ⁶N. Thillosen, Th. Schäpers, N. Kaluza, H. Hardtdegen, and V. A. Guzenko, *Appl. Phys. Lett.* **88**, 022111 (2006).
- ⁷N. Thillosen, S. Cabanas, N. Kaluza, V. A. Guzenko, H. Hardtdegen, and Th. Schäpers, *Phys. Rev. B* **73**, 241311(R) (2006).
- ⁸S. Schmult, M. J. Manfra, A. Punnoose, A. M. Sergent, K. W. Baldwin, and R. J. Molnar, *Phys. Rev. B* **74**, 033302 (2006).
- ⁹C. Kurdak, N. Biyikli, U. Ozgur, H. Morkoc, and V. I. Litvinov, *Phys. Rev. B* **74**, 113308 (2006).
- ¹⁰R. Winkler, *Spin Orbit Coupling Effects in Two-Dimensional*

Electron and Hole Systems (Springer-Verlag, Berlin, 2003).

- ¹¹V. I. Litvinov, *Phys. Rev. B* **68**, 155314 (2003).
- ¹²S. Hikami, A. I. Larkin, and Y. Nagaoka, *Prog. Theor. Phys.* **63**, 707 (1980).
- ¹³G. Bergmann, *Phys. Rep.* **107**, 1 (1984).
- ¹⁴G. M. Gusev, Z. D. Kvon, and V. N. Ovsyuk, *J. Phys. C* **17**, L683 (1984).
- ¹⁵A. G. Mal'shukov, K. A. Chao, and M. Willander, *Phys. Rev. B* **56**, 6436 (1997).
- ¹⁶A. G. Mal'shukov, V. A. Frolov, and K. A. Chao, *Phys. Rev. B* **59**, 5702 (1999).
- ¹⁷G. M. Minkov, A. V. Germanenko, O. E. Rut, A. A. Sherstobitov, L. E. Golub, B. N. Zvonkov, and M. Willander, *Phys. Rev. B* **70**, 155323 (2004).
- ¹⁸F. E. Meijer, A. F. Morpurgo, T. M. Klapwijk, T. Koga, and J. Nitta, *Phys. Rev. B* **70**, 201307(R) (2004).
- ¹⁹F. E. Meijer, A. F. Morpurgo, T. M. Klapwijk, and J. Nitta, *Phys. Rev. Lett.* **94**, 186805 (2005).
- ²⁰P. M. Mensz and R. G. Wheeler, *Phys. Rev. B* **35**, 2844 (1987).
- ²¹P. M. Mensz, R. G. Wheeler, C. T. Foxon, and J. J. Harris, *Appl. Phys. Lett.* **50**, 603 (1987).
- ²²H. Mathur and H. U. Baranger, *Phys. Rev. B* **64**, 235325 (2001).
- ²³V. I. Fal'ko, *J. Phys.: Condens. Matter* **2**, 3797 (1990).

- ²⁴M. V. Budantsev, Z. D. Kvon, A. G. Pogosov, and A. Tybulewicz, *Sov. Phys. Semicond.* **26**, 879 (1992).
- ²⁵J. S. Meyer, A. Altland, and B. L. Altshuler, *Phys. Rev. Lett.* **89**, 206601 (2002).
- ²⁶M. W. Bayerl, M. S. Brandt, T. Graf, O. Ambacher, J. A. Majewski, M. Stutzmann, D. J. As, and K. Lischka, *Phys. Rev. B* **63**, 165204 (2001).
- ²⁷S. V. Iordanskii, Y. B. Lyanda-Geller, and G. E. Pikus, *JETP Lett.* **60**, 206 (1994).
- ²⁸V. C. Dugarev and D. E. Khmel'nitskii, *Sov. Phys. JETP* **59**, 1038 (1984).
- ²⁹B. L. Al'tshuler and A. G. Aronov, *JETP Lett.* **33**, 499 (1981).